Chemical Communications RSCPublishing

COMMUNICATION

Cite this: DOI: 10.1039/x0xx00000x

Received 00th January 2014,
Accepted 00th January 2014

DOI: 10.1039/x0xx00000x

www.rsc.org/

Additive-free synthesis of V_4O_7 hierarchical structure as high performance cathode for lithium ion battery†‡

Xinran.Wang[ab], Shili.Zheng[a], Xuechao Mu[c], Yi.Zhang[a] and Hao.Du[a]*

Vanadium oxide (VO_x) hierarchical structures were controllably synthesized through a solvothermal method in water/ethylene glycol (EG) mixed media. A V_4O_7 "nanocross" structure is first reported and observed to exhibit exceptional cycling stability at 0.05 A.g^{-1} and 3.05 A.g^{-1}, which could be a promising cathode candidate for lithium ion battery.

Owing to its large theoretical capacity (~300 mAh.g^{-1}), vanadium oxide (VO_x) has long been considered as one of the most promising cathode material for lithium ion batteries (LIBs).[1-4] Unfortunately, its intrinsic disadvantages regarding poor structural stability and low lithium ion diffusion kinetics, severely limits its long-term performance with undesirable fast capacity fading. And the reason attributed to the instability was revealed to be the repeated lattice distortion that makes the structure breaking down upon cycling.[5-7] In recent years, structure manipulation is proven to be effective in improving VO_x cycling behavior, because such operation could significantly increase the electrochemical kinetics, shorten lithium ion penetration pathway and, to the most important, buffer lattice expansion during the charge/discharge process.[8-10] Consequently, VO_x nanostructures in the form of nanofibers,[11, 12] nanoribbons[13, 14] and nanowires[15, 16] have been extensively studied. However, nanoparticles inevitably agglomerate due to the low thermodynamic stability. The agglomeration creates the isolation between particles and conductive agent, giving rise to the increase of polar intensity and electron transfer resistance. More recently, VO_x hierarchical architecture has attracted great attention, because it provides organizations that could prevent particles self-aggregation upon cycling.[12, 17-27] In this regards, much progress on synthesizing hierarchical VO_x has been reported in literatures, among which hydrothermal or solvothermal method appears to be the most effective due to the high repeatability. However, when hydrothermal or solvothermal procedure is applied, controlling the orientation of molecules is a necessity for the growth of regular hierarchical structure. Additives, such as templating polymers, are commonly used whereas template-free synthesis appears to be a challenge due to the difficulty in effectively controlling the structure.

Ethylene glycol (EG) has been widely applied as a solvothermal media for the hierarchical structure synthesis, and in most cases, combined with templating polymer, such as polyvinyl pyrrolidone (PVP) and hexadecyl trimethyl ammonium bromide (CTAB).[28-30] In particular, Uchaker sets a good example on effectively synthesizing hollow hierarchical VO_x structure with EG.[31] The pure EG media creates a hollow microsphere, which is built up by nanoribbons, and exhibits improved cycling performance. Furthermore, the mechanism of solvothermal process in the presence of EG has been proposed and summarized as follows: (1) the formation of metal glycolate through the coordination of EG and central metal ion; (2) subsequent oligomerization. Nevertheless, limited research has reported other structure rather than hollow microsphere or core-shell structure. And the cycling performance of VO_x hierarchical structure is not as stable as desired.

Herein, water/EG mixed solvent was applied as the solvothermal media for synthesizing VO_x hierarchical structure. The morphology was revealed to be controlled without any additive. And the amount of water in EG solvent triggered the morphology and crystallinity transfer, giving rise to a series of distinct VO_x hierarchical structures. In particular, a novel structure of V_4O_7 "nanocross" was originally synthesized and found with exceptional cycling stability as cathode for LIBs. A capacity of 305.6 mAh.g^{-1} has been achieved and maintained at 0.05 A.g^{-1}. Moreover, V_4O_7 "nanocross" also exhibits stable cycling performance at 3.05 A.g^{-1} with a reversible capacity of 176 mAh.g^{-1} and 100 % capacity retention. The crystallinity and morphology of VO_x hierarchical structures are carefully compared and found critical to their cycling performance, as suggested by galvanostatic measurement.

The detailed synthesis procedure of hierarchical VO_x can be found in the ESI. A series of VO_x hierarchical structure was harvested by consequently increasing water content in the mixed media. The harvested products were directly characterized by field-emission scanning electron microscope (FESEM) as shown in Figure 1 and Fig. S1. In pure EG solvent (Fig. 1A), a microsphere structure was created, which is built up by regular nanoparticles with diameter

[a] National Engineering Laboratory for Hydrometallurgical Cleaner Production Technology, Key Laboratory of Green Process and Engineering, Institute of Process Engineering, Chinese Academy of Sciences, Beijing, Box 353
[b] University of Chinese Academy of Sciences, No.19A Yuquan Road, Beijing
[c] College of Chemical Engineering, Beijing University of Chemical Technology, Beijing

less than 50 nm (Fig. S2). When water content was increased to 12.5 % (Fig. 1B), nanoparticles aggregation turned out to be dispersed and some grew to nanoribbons due to the condensation of VO*x*. Therefore, a composition of nanoribbons and nanoparticles was obtained. Further increasing water content to 25 %, a unique structure characterized as "nanocross" was obtained, in which plate-shape architecture is formed and many plates even crossed another in the middle (Fig. 1C). With 75% water content, the VO*x* nanosheet self-aggregated to a flower-shape structures (Fig. 1D) whereas 94 % water gave rise to the structure of microsphere (Fig. 1E).

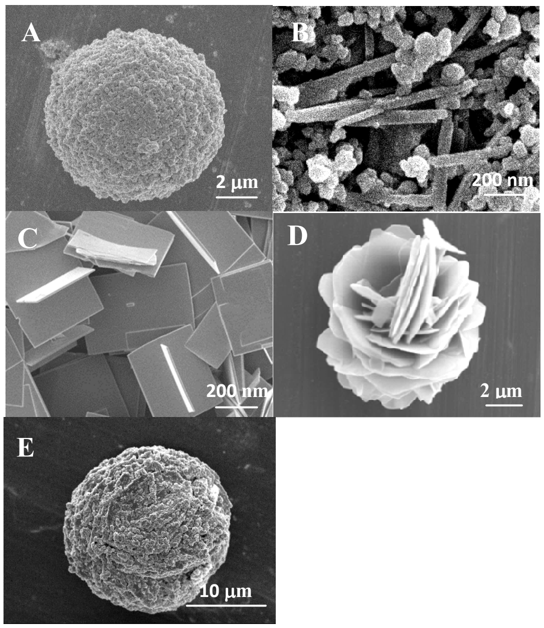

Fig. 1 Morphological characterization of VO_x hierarchical structure with (A) 0 %, (B) 12.5 %, (c) 25%, (D) 75 % and (E) 95 % water content.

Their crystallinities were collected and compared in Fig. 2. In pure EG, product of typical VO_2 (B) was obtained, indexed to JCPDS: 81-2392 (Fig. 2A). In an anhydrous EG solution, the precursor reacted with EG to form the metal glycolate and it oligomerized during the solvothermal process. Meanwhile, EG is reported to be a reductive agent, which would be oxidized to glyoxal at 180 ^oC. Furthermore, the dissolved ammonium could increase the reducibility. Hence, the reductive media is attributed to the change of vanadium valence. For samples with 12.5 % and 25 % water content, an increasing growth of V_4O_7 crystallinity was illustrated. In particular, the "nanocross" with 25 % water content exhibited a significantly preferred (001) growth orientation of V_4O_7 crystallinity, indexed to JCPDS: 65-6448. The XRD tests reveals that a solvothermal media with an appropriate water/EG ratio can produce different VO*x* crystallinity. In mixed solution, EG could react with vanadium oxide precursor only through glycolation process. However, water could not only react with vanadium oxide precursor through hydrolysis process, but also intercalates into the double layer to form VO*x* hydrogel. Due to the low water content (0%, 12 % and 25%), more precursor tended to react with EG to create VO_2(B) or V_4O_7. The low water content is not sufficient to give rise to amorphous double-layer VO*x* hydrogel. The structure of ordered V_4O_7 crystallinity was further evaluated by TEM images (Fig. S3). TEM image in Fig. S3A illustrates a 2D nanosheet with another small piece of sheet perpendicularly grown in the central of the previous one. High resolution TEM (Fig. S3B) exhibits an exposure of (001) crystal phase with 1 nm layer distance. Nevertheless, based on our observation, when water content was in excess of 50 %, the XRD results indicated the formation of amorphous VO*x* hydrogel (Fig. S4). According to the literature, the vanadium oxide gel has a long-term disordered arrangement with short-term bi-layer structure, and thus exhibits amorphous structure as integrity. In general, the morphology difference upon change of EG/water ratio is considered to be derived from both the product crystallinity and the polarity difference between water and EG. To be specific, in pure EG, the precursor could only undergo glycolate process to form nanoparticles. Due to the high surface energy, these nanoparticles turned to aggregate to microsphere. The vanadium (V) is reduced to vanadium (IV) with the oxidation of EG, giving rise to a pure VO_2 crystallinity. However, with 12.5 % and 25 % water content, V_4O_7 crystallinity gradually formed, which exhibited critical preferred (001) crystal phase. In this circumstance, we believe that the morphology change is due to the V_4O_7 formation. As for high water content of 75 % and 95 %, the low content of EG would form a complicated quasi-emulsion system due to the polarity difference, which could control the morphology.

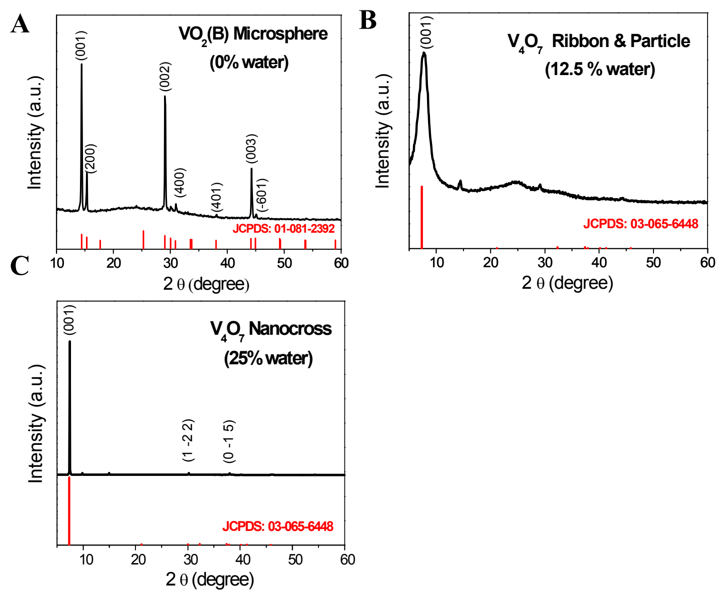

Fig. 2 Crystallinity characterization of VOx hierarchical structure with (A) 0 %, (B) 12.5 %, (c) 25% water content.

To demonstrate the potential VO_x application, we investigated their cathode performance in lithium ion batteries. The cathode capacity of the hierarchical VO_x, in terms of lithium ion storage, was evaluated by galvanostatic charge/discharge measurement. All the as-prepared products were directly assembled into the coin cell and cycled between 1.5 and 4.0 V at 50 $mA.g^{-1}$. The cycling performance of VO_x hierarchical structures under different water content was illustrated in Fig. 3. Among all the structures, V_4O_7 "nanocross" (25 % water content) exhibits the highest capacity with exceptional cycling stability. It achieved a reversible capacity of 305.6 $mAh.g^{-1}$ after 100 cycles, 95 % of its initial discharge capacity. In the term of other hierarchical structures, samples under 0 % and 12.5 % water content all exhibit high initial capacity (458 and 400 $mAh.g^{-1}$, respectively) whereas the 100 cycles performances kept only 24 % and 34 % of its initial capacity. Amorphous structures (including products under 75 % and 94 % water content) maintained 50 % and 36 % of their initial capacity after 100 cycles. The distinct cycling stability is considered to be derived from the crystallinity difference. And the formation of V_4O_7 significantly increased the cycling stability. The unique structure make a dominant orientation growth along *c* axis, where lithium ions is considered to intercalate into the structure.[32] As a comparison of their first-cycle discharge (Fig. S5), nanocross delivered 83 % of its total discharge capacity above 2.3 V, higher than other VO_x hierarchical structures. Products under 12.5 % water content, which also contains V_4O_7 crystallinity, shows similar discharge plateau whereas other products exhibit almost linear discharge curves. The difference on discharge behavior indicates that V_4O_7 promotes fast lithium ion intercalation with relatively low polar density. Improved stability of V_4O_7 nanocross is further illustrated by the detailed charge/discharge curves as shown in Fig. 3B. It demonstrates that the charge process maintains during the 100 cycle. However, an additional small plateau around 1.6 V became apparent after fiftieth discharge cycle, corresponding to ~50 $mAh.g^{-1}$ capacity. Due to the formation of the plateau, the capacity obtained at 100 th. cycle even surpassed that of 10 th. cycle. After 100 cycles, still 71 % of total discharge capacity has been delivered at plateau above 2.3 V. The corresponding rate performance of "nanocross" V_4O_7 was shown in Fig. S6. It delivered 291, 261, 209, 186 and 159 $mAh.g^{-1}$ cycled at 0.05, 0.1, 1, 2, 3 $A.g^{-1}$, respectively. Additional 5 cycles at 0.05 $A.g^{-1}$ was conducted to evaluate the capacity resumption ability. It reached to 290 $mAh.g^{-1}$, an indication of good resumption. Fig. S6B displayed charge/discharge profile of each current density, which shows a consistent discharge performance with 2.4 V plateau.

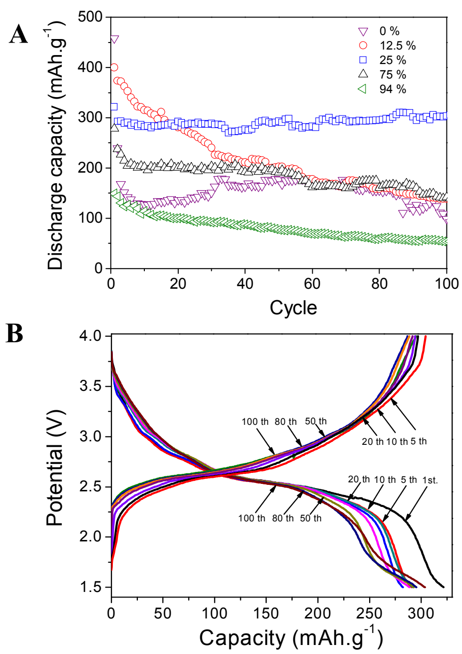

Fig. 3 Cycling performance of hierarchical VO*x* synthesized with different water content: (A) 100 cycles charge/discharge performance at 50 $mA.g^{-1}$; (B) corresponding discharge profiles of 100 cycles of V_4O_7 nanocross.

In order to elucidate the redox reaction during the lithium ion insertion/extraction process, CV test of V_4O_7 nanocross was carried out and the results is shown in Fig. 4. CV profiles of the first, fiftieth, and one hundredth cycles were compared. The comparison suggests a stable electrochemical redox behavior with multiple lithium ion insertion/extraction steps. During the lithium ion extraction, the major anodic peak located around 3.1 V was observed. The corresponding cathodic peak was located at 2.4 V with several minor peaks around 2.7 V-3.5 V. In accordance with literature, these redox peaks demonstrated a two-phase V(IV)/ V(III) changes upon the lithiumation/delithiumation process. However, no redox peak of V_2O_3 for V(III)/ V(II) was observed.[33-36] Based on the data collected from CV test, we deduced that only the VO_2 layer in V_4O_7 functionalized as the site for lithium ion insertion. Suggested by the charge/discharge investigation in this study, the discharge capacity of 305.6 $mAh.g^{-1}$ for V_4O_7 cycled at 50 $mA.g^{-1}$ indicated a 3.6 lithium ions insertion. The reaction was thus tentatively deduced as follow:

$$V_4O_7 + 3.6Li^+ + 3.6e^- \longrightarrow Li_{3.6}V_4O_7$$

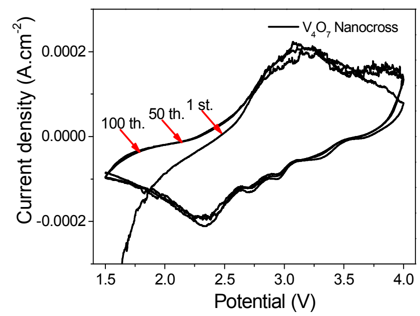

Fig. 4 CV test of V_4O_7 nanocross under 0.5 $mV.s^{-1}$ current density.

EIS measurements were carried out for the comparison of electrochemical properties of sample with different water content, as shown in Table 1 and Fig. S7. Among all the hierarchical VO*x*, "nanocross" exhibits significantly improved electrochemical resistance (R_{st}) as suggested by the hemi-circle at high frequency area. The low R_{st} can improve the polar density, which further influences the charge/discharge behavior. The Warburg coefficient and lithium ion diffusion coefficient were quantitatively measured (Fig. S8, SI Equation (1) and Equation (2)) and summarized in Table 1. Different hierarchical VO*x* shows similar lithium ion diffusion coefficient. However, "nanocross" has the lowest electrochemical resistance, which indicated that lithium ions are much easier to insert into "nanocross" crystallinity and react with V_4O_7. This advantage is attributed to the better cycling performance and may give rise to a promising rate performance.

Table 1 Summary of electrochemical properties of hierarchical VO*x* with different water content

Water content %	R_e/Ω	$R_{ct}+R_{SEI}/\Omega$	$\sigma_w/\Omega\ s^{-0.5}$	$D/cm^2\ s^{-1}$
0	19.6	677	20	1.47842×10^{-9}
12.5	7.56	453	22.5	1.30526×10^{-9}
25	16.6	238	25	1.16531×10^{-9}
75	13	1017	18	1.67162×10^{-9}
95	11.7	1168	19	1.57835×10^{-9}

To further illustrate the rate stability of V_4O_7 nanocross, its cycling performance under high current density of 3.05 $A.g^{-1}$ was performed and shown in Fig. 5. Even at high current density, V_4O_7 nanocross exhibits exceptional cycling stability, delivering reversible capacity of 175.5 $mAh.g^{-1}$ at the 100 cycle. The galvanostatic tests suggested a 100 % of capacity retention. The much improved stability at high rate is derived from the unique V_4O_7 structure with much less electrochemical resistance and low polar density. The corresponding charge/discharge profile is shown in Fig. S9, which reveals that the capacity of 100 cycles even surpasses that obtained from initial cycle. Such phenomenon indicates that V_4O_7 nanocross needs an activation process to ensure the sufficient reversible lithium ion insertion at high rate.

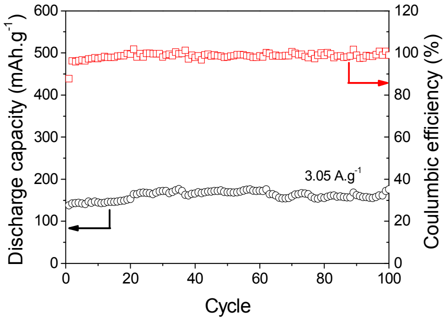

Fig. 5 Cycling performance of V_4O_7 nanocross at high rate: (A) galvanostatic test of V_4O_7 nanocross under 3.05 A.g^{-1}; (B) corresponding discharge profiles of 100 cycles

The unique structure of V_4O_7 nanocross was first synthesized through solvothermal procedure in a mixed water/ EG media. In comparison with other hierarchical structures, the V_4O_7 nanocross exhibits large amount of (001) crystal plane which could be the channel of lithium ion insertion. Therefore, a much improved cycling stability was demonstrated of the V_4O_7 nanocross lithium ion storage. Capacity of 305.6 mAh.g^{-1} was obtained and maintained at 0.05 A.g^{-1}. Its cycling performance at high rate of 3.05 A.g^{-1} also demonstrates a stable cycling performance with 100% capacity retention of 175.5 mAh.g^{-1}. Therefore, V_4O_7 nanocross is considered to be a promising candidate as cathode for lithium ion battery.

Notes and references

†Electronic supplementary data (ESI) available: see….

‡*Preparation*: The VO_x hierarchical structure was prepared by a facile solvothermal method in a mixed water/ethylene glycol (EG) solvent (Sigma-Aldrich). In a typical synthesis, 10 ml water was mixed with 70 ml (EG). Subsequently, 0.1 g NH_4VO_3 (Sigma-Aldrich) was added into the mixed solvent with ultrasonic for 1 h. And then the mixture was transferred into a 200 ml Teflon-lined stainless steel autoclave. The autoclave was heated at 180°C for 24h and cooled down to room temperature naturally. The as-prepared powder was separated by centrifugation, washed with water and absolute ethanol several times and dried in 80 °C oven over night.

Characterization: The samples were characterized using X-Ray diffraction (XRD, Panalytical, X'Pert PRỌẠ-1 diffractometer, Cu-KẠ), transmission electron microscopy (TEM, JEOL,JEM-2100F), energy dispersive X-ray spectroscopy (EDX,FEI, MLA 250), field-emission scanning electron microscope (FESEM, JEOL,JEM2100).

The electrochemical properties were evaluated using two electrodes 2025 coin cell with lithium metal disks as the counter and reference electrode. The cathode consisted of the prepared VO_x, acetylene black and poly(vinylidene difluoride) in the ratio of 80:10:10. Polypropylene membrane (Celgard, 2400) was used as separator(Ạ20 mm). The electrolyte used was 1 M $LiPF_6$ dissolved in 1:1 V/V ethylene carbonate/dimethyl carbonate (EC/DMC) solvent. The cyclic voltammetry (CV) and electrochemical impedance spectroscopy (EIS) were tested on ModuLab station and galvanostatic charge-discharge properties were evaluated using a LAND battery system (CT2001A).

1. Y. Wang and G. Z. Cao, *Advanced Materials*, 2008, **20**, 2251-2269.
2. Y. Sakurai, S. Okada, J. Yamaki and T. Okada, *Journal of Power Sources*, 1987, **20**, 173-177.
3. V. Petkov, P. N. Trikalitis, E. S. Bozin, S. J. L. Billinge, T. Vogt and M. G. Kanatzidis, *Journal of the American Chemical Society*, 2002, **124**, 10157-10162.
4. Y. Wang and G. Cao, *Advanced Materials*, 2008, **20**, 2251-2269.
5. B. Scrosati, *J. Electrochem. Soc.*, 1992, **139**, 2776-2781.
6. C. J. Patrissi and C. R. Martin, *J. Electrochem. Soc.*, 1999, **146**, 3176-3180.
7. J. W. Lee, S. Y. Lim, H. M. Jeong, T. H. Hwang, J. K. Kang and J. W. Choi, *Energy & Environmental Science*, 2012, **5**, 9889-9894.
8. C. R. Sides and C. R. Martin, *Advanced Materials*, 2005, **17**, 125-+.
9. S. Q. Wang, S. R. Li, Y. Sun, X. Y. Feng and C. H. Chen, *Energy & Environmental Science*, 2011, **4**, 2854-2857.
10. L. Q. Mai, Q. L. Wei, Q. Y. An, X. C. Tian, Y. L. Zhao, X. Xu, L. Xu, L. Chang and Q. J. Zhang, *Advanced Materials*, 2013, **25**, 2969-2973.
11. Y. Wang, K. Takahashi, K. Lee and G. Z. Cao, *Advanced Functional Materials*, 2006, **16**, 1133-1144.
12. L. Q. Mai, L. Xu, C. H. Han, X. Xu, Y. Z. Luo, S. Y. Zhao and Y. L. Zhao, *Nano Letters*, 2010, **10**, 4750-4755.
13. Y. Wang and G. Z. Cao, *Chemistry of Materials*, 2006, **18**, 2787-2804.
14. Y. Shi, S. L. Chou, J. Z. Wang, H. J. Li, H. K. Liu and Y. P. Wu, *Journal of Power Sources*, 2013, **244**, 684-689.
15. X. L. Jia, Z. Chen, A. Suwarnasarn, L. Rice, X. L. Wang, H. Sohn, Q. Zhang, B. M. Wu, F. Wei and Y. F. Lu, *Energy & Environmental Science*, 2012, **5**, 6845-6849.
16. J. S. Ke, S. F. Weng, M. C. Wu and C. S. Lee, *Journal of Nanoparticle Research*, 2013, **15**.
17. H. C. Pang, P. Cheng, H. B. Yang, J. L. Lu, C. X. Guo, G. L. Ning and C. M. Li, *Chemical Communications*, 2013, **49**, 1536-1538.
18. A. M. Cao, J. S. Hu, H. P. Liang and L. J. Wan, *Angewandte Chemie-International Edition*, 2005, **44**, 4391-4395.
19. C. Z. Wu, Y. Xie, L. Y. Lei, S. Q. Hu and C. Z. OuYang, *Advanced Materials*, 2006, **18**, 1727.
20. D. Sun, C. W. Kwon, G. Baure, E. Richman, J. MacLean, B. Dunn and S. H. Tolbert, *Advanced Functional Materials*, 2004, **14**, 1197-1204.
21. S. D. Zhang, Y. M. Li, C. Z. Wu, F. Zheng and Y. Xie, *Journal of Physical Chemistry C*, 2009, **113**, 15058-15067.
22. H. M. Liu and W. S. Yang, *Energy & Environmental Science*, 2011, **4**, 4000-4008.
23. A. Q. Pan, H. B. Wu, L. Yu, T. Zhu and X. W. Lou, *Acs Applied Materials & Interfaces*, 2012, **4**, 3874-3879.
24. A. Q. Pan, H. B. Wu, L. Zhang and X. W. Lou, *Energy & Environmental Science*, 2013, **6**, 1476-1479.
25. B. H. Wu, A. Q. Pan, H. H. Hng and X. W. Lou, *Advanced Functional Materials*, 2013, **23**, 5669-5674.
26. A. Q. Pan, T. Zhu, H. B. Wu and X. W. Lou, *Chemistry-a European Journal*, 2013, **19**, 493-499.
27. A. Pan, H. B. Wu, L. Yu and X. W. Lou, *Angewandte Chemie International Edition*, 2013, **52**, 2226-2230.
28. S. Lv, C. Wang and X. T. Yang, *Micro & Nano Letters*, 2013, **8**, 234-237.
29. K. L. Harrison and A. Manthiram, *Chemistry of Materials*, 2013, **25**, 1751-1760.
30. J. J. Zhang, Y. Yao, T. Huang and A. S. Yu, *Electrochim. Acta*, 2012, **78**, 502-507.
31. E. Uchaker, N. Zhou, Y. Li and G. Cao, *The Journal of Physical Chemistry C*, 2013, **117**, 1621-1626.
32. A. S. Botana, V. Pardo, D. Baldomir, A. V. Ushakov and D. I. Khomskii, *Physical Review B*, 2011, **84**.
33. H. Liu, Y. Wang, K. Wang, E. Hosono and H. Zhou, *Journal of Materials Chemistry*, 2009, **19**, 2835-2840.
34. Y. Liu, E. Uchaker, N. Zhou, J. Li, Q. Zhang and G. Cao, *Journal of Materials Chemistry*, 2012, **22**, 24439-24445.
35. N. Li, W. Huang, Q. Shi, Y. Zhang and L. Song, *Ceramics International*, 2013, **39**, 6199-6206.
36. Q. Zhao, L. Jiao, W. Peng, H. Gao, J. Yang, Q. Wang, H. Du, L. Li, Z. Qi, Y. Si, Y. Wang and H. Yuan, *Journal of Power Sources*, 2012, **199**, 350-354.